Supplementary Materials for

Thermally activated growth of ternary oxyhydroxides on perovskite for efficient water oxidation

Authors: Chao Wu,[ab] Zhanhong Xiao,[a] Ying Tang,[a] Junhua Li,[a] Anqi Zou,[a] Jiliang Zhu,[a] Xiaopeng Wang,*[ac] and Jiagang Wu*[a]

Affiliations:

[a] College of Materials Science and Engineering, Sichuan University, Chengdu, 610065, China.

[b] Institute of Sustainability for Chemical, Energy and Environment (ISCE^2), Agency for Science, Technology and Research (A*STAR), 1 Pesek Road Jurong Island, Singapore, 627833, Republic of Singapore.

[c]State Key Laboratory of Intelligent Construction and Healthy Operation and Maintenance of Deep Underground Engineering, Sichuan University, Chengdu, 610065, China.

*Correspondence to: wangxiaopeng@scu.edu.cn (Xiaopeng Wang);
wujiagang0208@163.com (Jiagang Wu);

This PDF file includes:

Methods and Characterization

Material synthesis.

$Sr_3Co_2WO_9$ (SCWO), $Sr_3CoFeWO_9$ (SCFWO), $Sr_3Co_{1.5}Fe_{0.5}WO_9$, $Sr_3Co_{0.5}Fe_{1.5}WO_9$ and $Sr_3Fe_2WO_9$ samples were synthesized by sol-gel methods within this work.[1] Firstly, the metal precursors $Sr(NO_3)_2$, $Co(NO_3)_2$, $Fe(NO_3)_2$ and WCl_6 were mixed in stoichiometric ratio with distilled water (DI). Next, the metal solution was mixed with Citric Acid (CA) and Ethylene Diamine Tetra acetic Acid (EDTA) with molar ratio of 1:1:1.5 by magnetic stirring. After that, the pH value of the obtained solution was adjusted to ~7 by the addition of ammonia solution (25 wt%), and the solution was continuously stirred at 90 ℃ for 6 hours to obtain the sol. Then, the obtained wet sol was transferred into a Al_2O_3 crucible and kept at 180 ℃ in a vacuum to yield dried gel. Finally, the dried gel was grinded into powder and annealed at 700-1000 ℃ in a muffle furnace under air atmosphere for 4 hours, and the final products can be collected after grinding the annealed powder.

Electrochemical measurements.

In this work, the working electrodes for electrochemical measurements were prepared by ink drop casting method. In brief, 15 mg of catalysts were ultrasonic dispersed in 3 mL ethanol firstly, and then 60 μL of Nafion solution (5%, Aladdin) was dropped into the above dispersion. Finally, 15 μL of the final mixed ink was drop casted onto finely polished glassy carbon electrode (0.0706 cm^2 in projected surface area) and dried in natural environment. Then, the electrochemical measurements were conducted on a three-electrode system connected to an electrochemical workstation (CHI 760E, CH instruments). The reference electrode was a Hg/HgO electrode, which was calibrated prior to the electrochemical experiments. A Pt foil served as the counter electrode, and the catalyst-laden ink-casted glassy carbon (GC) electrode was applied as the working electrode. Conversion between the potentials versus RHE and versus Hg/HgO was carried out with the following equation: E (versus RHE) = E (versus Hg/HgO) + $E_{Hg/HgO}$ (versus standard hydrogen electrode (SHE)) + 0.059 × pH. The electrochemically active surface area (ECSA) of the electrodes was determined by double layer capacitance method. In this process, cyclic voltammetry (CV)

curves were obtained across the potential range of 1.04 to 1.14 V *vs*. RHE, with scan rates spanning 10-100 mV/s. And the double layer capacitance (C_{dl}) values were extracted by linear fitting the anodic current densities extracted from CV plots. The electrochemically active surface area (ECSA) was determined by the double layer capacitance (C_{dl}) according to the following equation: ECSA = C_{dl} / C_S, C_S value is adopted as 40 μF cm^{-2}, referencing the value of Ni surfaces in alkaline electrolytes.[2] The linear scan voltammetry (LSV) curves of all the samples were recorded in the range of 1.3-1.65 V *vs.* RHE in backward runs with scan rate of 5 mV/s in 1 M KOH electrolytes, no *iR* compensation was performed in the data extracting process. Chronopotentiometry (CP) measurements were performed on the reconstructed SCWO and SCFWO samples by maintaining a specific current density of 10 mA cm^{-2}_{geo} for 60 hours.

Material characterizations.

The powder X-ray Diffraction (PXRD) data for both the pristine and immersed samples were acquired using DX2700 diffractometer with Cu *Kα* radiation. To examine surface morphologies, a Regulus 8230 field emission scanning electron microscope (SEM, Hitachi) was utilized for all samples. Transmission Electron Microscopy (TEM), High-Resolution TEM (HRTEM) and energy dispersive spectroscopy (EDS) measurements were performed using a JEOL 3200F instrument operating at 200 kV. For X-ray Photoelectron Spectroscopy (XPS) measurements, a Thermo Scientific Escalab 250Xi electron spectrometer was employed, employing Al *Kα* X-rays ($h\nu$ = 1486.6 eV) as the excitation source.

XAS measurements.

Co *K*-edge, Fe *K*-edge and W L_3-edge X-ray absorption spectroscopy (XAS) spectra were collected at the XAFCA beamline of Singapore Synchrotron Light Sources (SSLS) using transmission mode,[3] and the data were processed according to the standard procedures in Athena module within the Demeter software packages.[4] For energy calibration, metal (Co, Fe, and W) foils were measured simultaneously with the samples. The EXAFS fitting was conducted in Artemis module using FEFF6 theoretical scattering path calculation code, the *k* range was set as 3-11 $Å^{-1}$, *R* range was set as 1-2.2 Å. Wavelet transform (WT) of the EXAFS data were conducted on Fortran software.

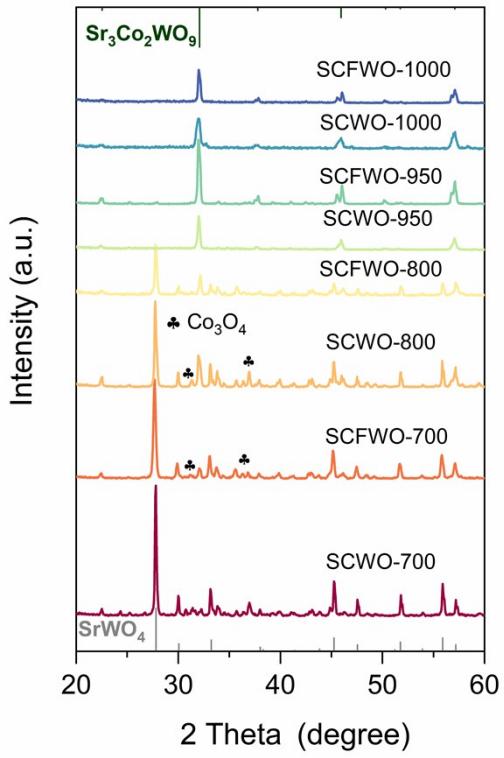

Supplementary Fig. 1. Powder X-ray diffraction (PXRD) patterns of $Sr_3Co_2WO_9$ (SCWO) and $Sr_3CoFeWO_9$ (SCFWO) samples calcined under 700, 800, 950 and 1000 ℃.

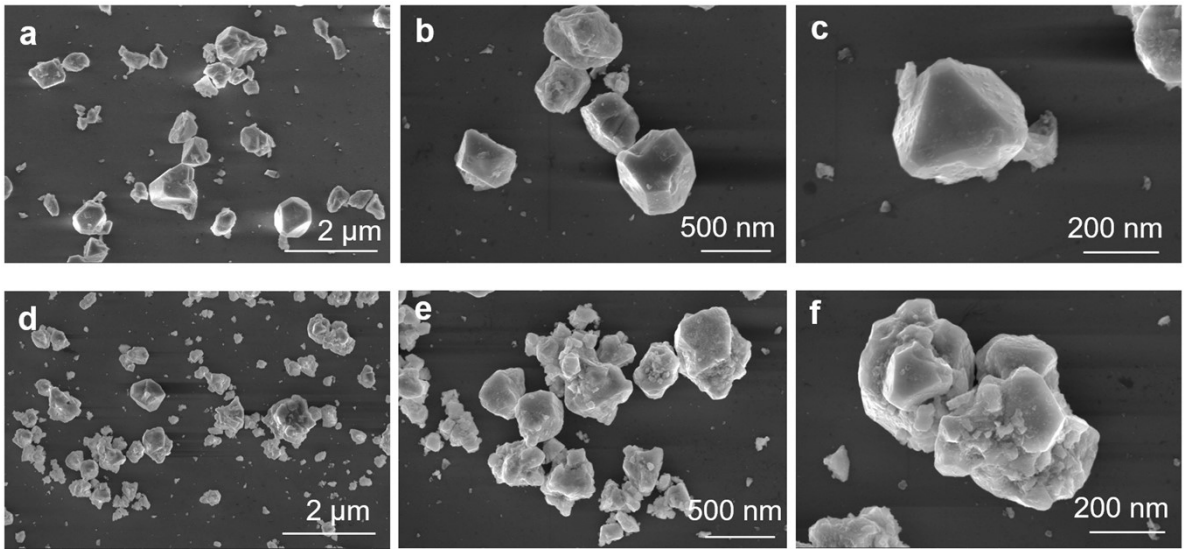

Supplementary Fig. 2. Scanning electron microscopy (SEM) images of (a-c) SCWO and (d-f) SCFWO samples calcined at 1000 ℃.

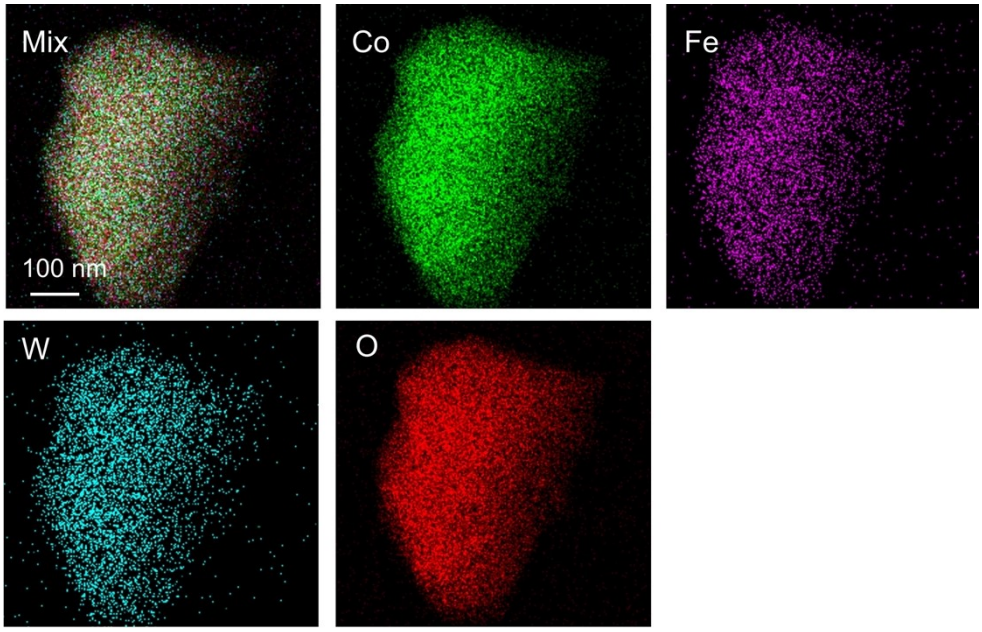

Supplementary Fig. 3. TEM energy dispersive spectroscopy (EDS) mapping of the SCFWO samples, including Co, Fe, W and O elements.

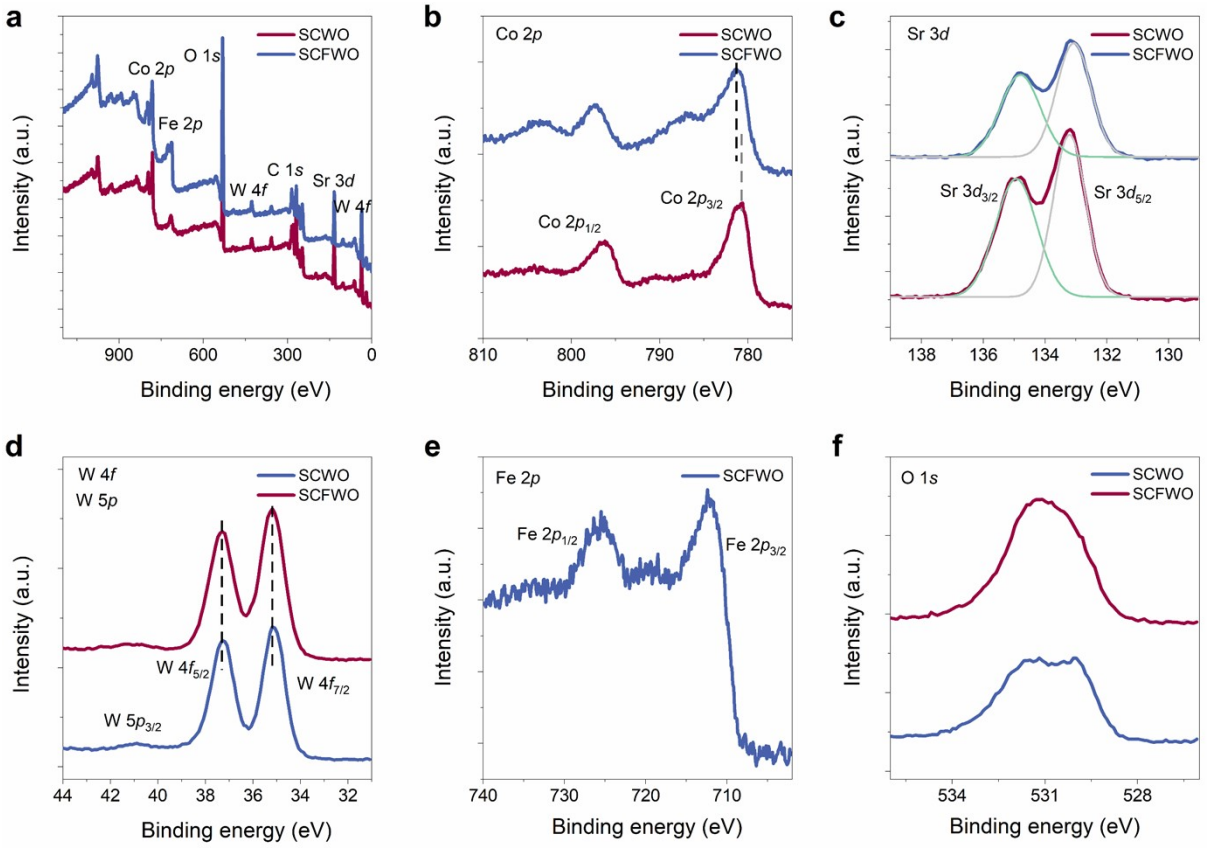

Supplementary Fig. 4. X-ray photoelectron spectroscopy (XPS) (a) survey scan, (b) Co 2*p*, (c) Sr 3*d*, (d) W4 *f*/5*p*, (e) Fe 2*p*, and (f) O 1*s* spectra of SCWO and SCFWO samples.

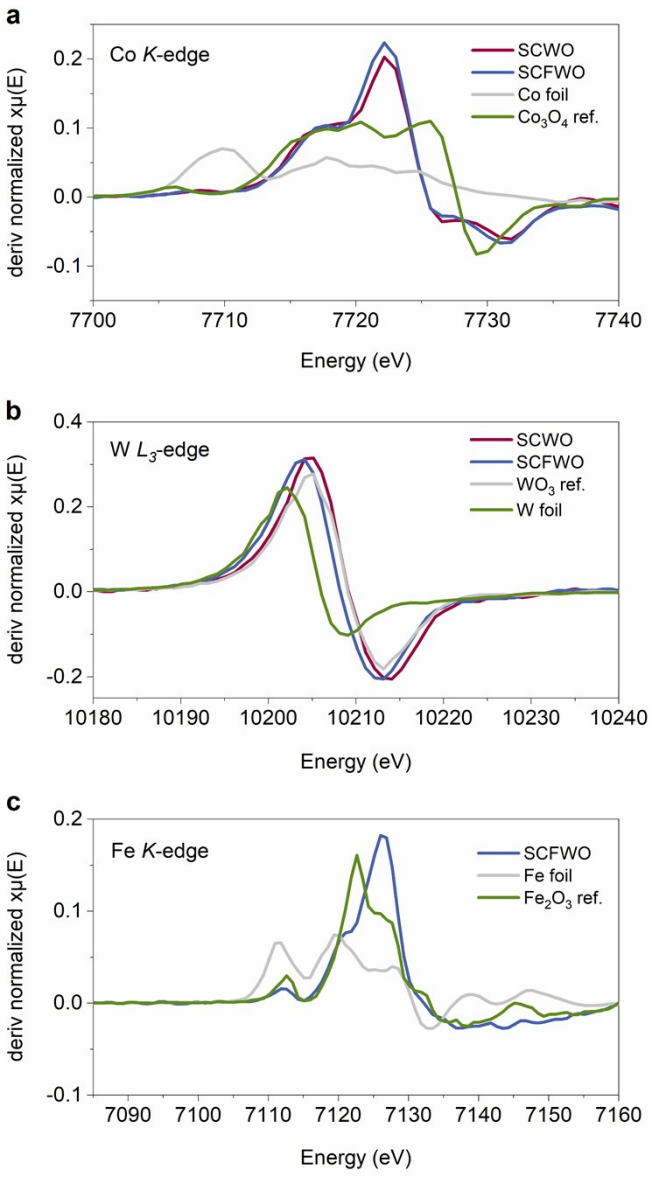

Supplementary Fig. 5. (a) First derivative for the normalized Co *K*-edge XANES spectra of SCWO and SCFWO samples, with Co_3O_4 and Co foil as reference. (b) First derivative for the normalized W L_3-edge XANES spectra of SCWO and SCFWO samples, with WO_3 and W foil as reference. (c) First derivative for the normalized Fe *K*-edge XANES spectra of SCFWO sample, with Fe_2O_3 and Fe foil as reference.

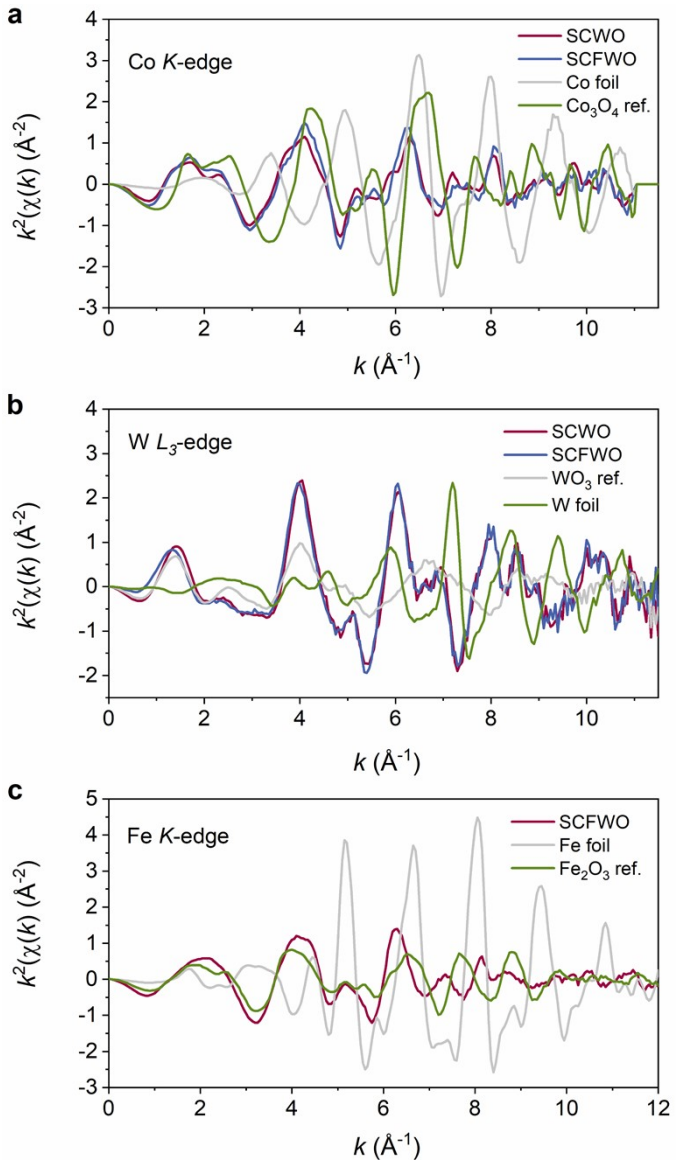

Supplementary Fig. 6. (a) *k*-space Co *K*-edge XAS spectra of SCWO and SCFWO samples, with Co_3O_4 and Co foil as reference. (b) *k*-space W L_3-edge XAS spectra of SCWO and SCFWO samples, with WO_3 and W foil as reference. (c) *k*-space Fe *K*-edge XAS spectra of SCFWO sample, with Fe_2O_3 and Fe foil as reference.

As shown in the *k* space XAS spectra, all these data exhibited a high signal-to-noise ratio, ensuring reliable analysis of the EXAFS data.

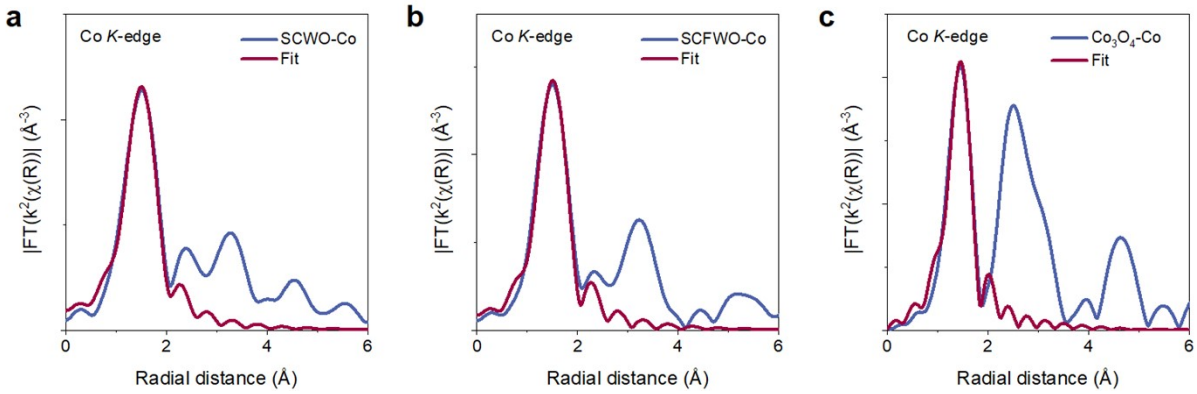

Supplementary Fig. 7. EXAFS fitting curves of Co *K*-edge spectra of (a) SCWO, (b) SCFWO and (c) Co_3O_4 samples.

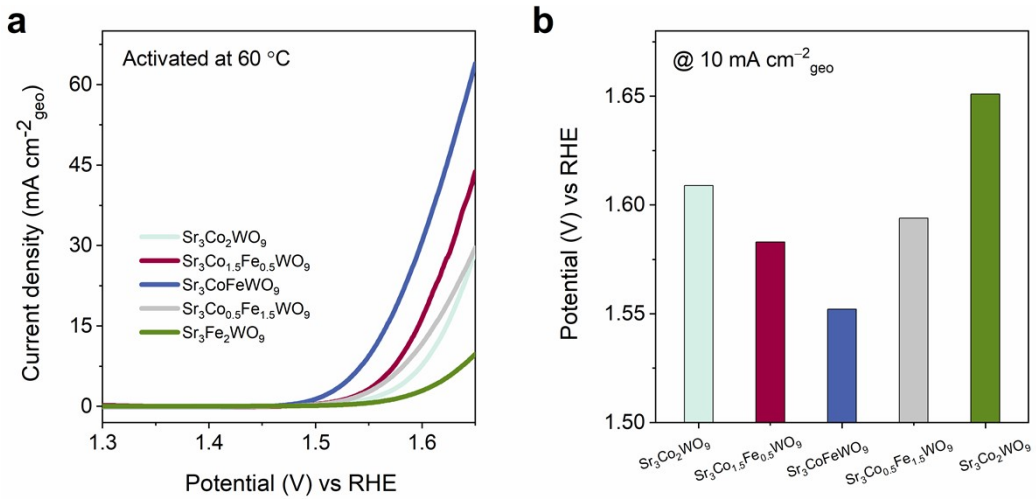

Supplementary Fig. 8. (a) Backward scan polarization curves (1.3-1.65 V *vs*. RHE) measured at 5 mV/s in 1M KOH electrolytes. (b) Required potential at 10 mA cm^{-2}_{geo} for the reconstructed perovskites (activated under 60 °C) with various ratios of Fe to Co.

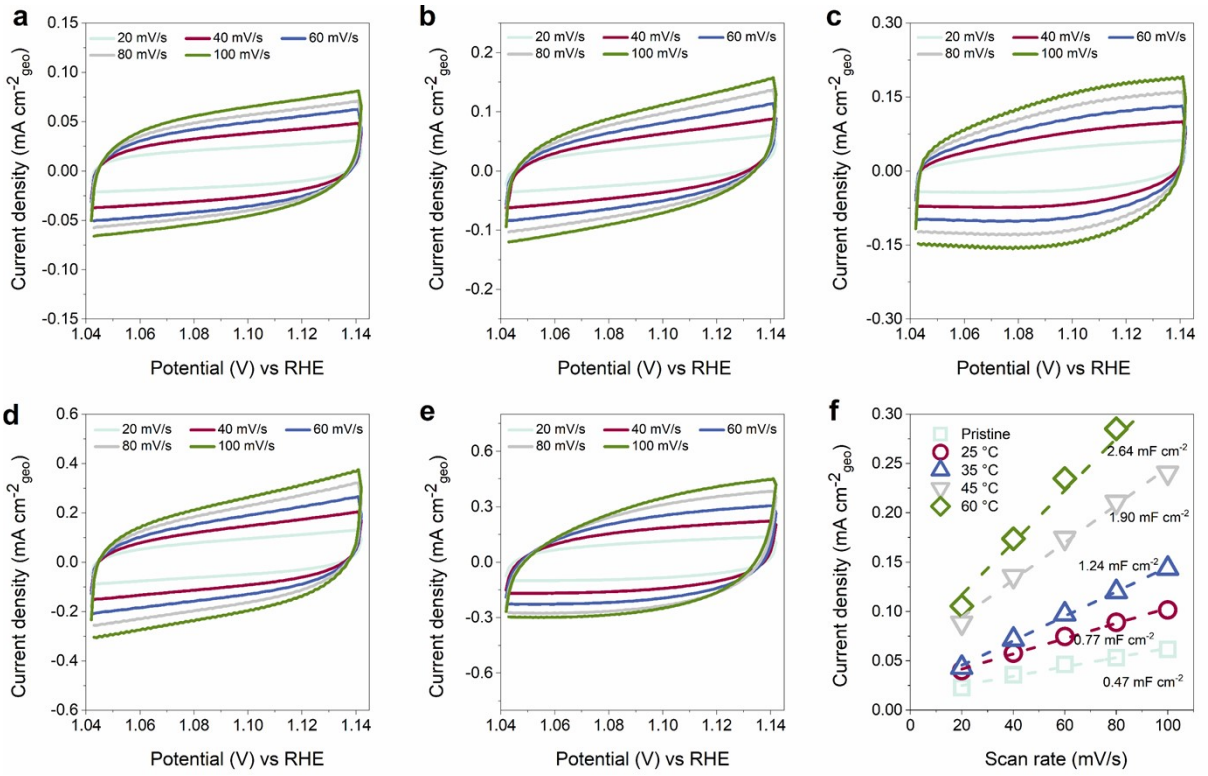

Supplementary Fig. 9. (a-e) Cyclic voltammetry (CV) scans with various scan rates (10-100 mV/s) in the non-faradic current range of 1.04 to 1.14 V *vs.* RHE for the pristine SCFWO sample and after being thermally activated at 25, 35, 45, and 60 °C, respectively. (f) Linear fitting of the anodic current densities extracted from CV plots.

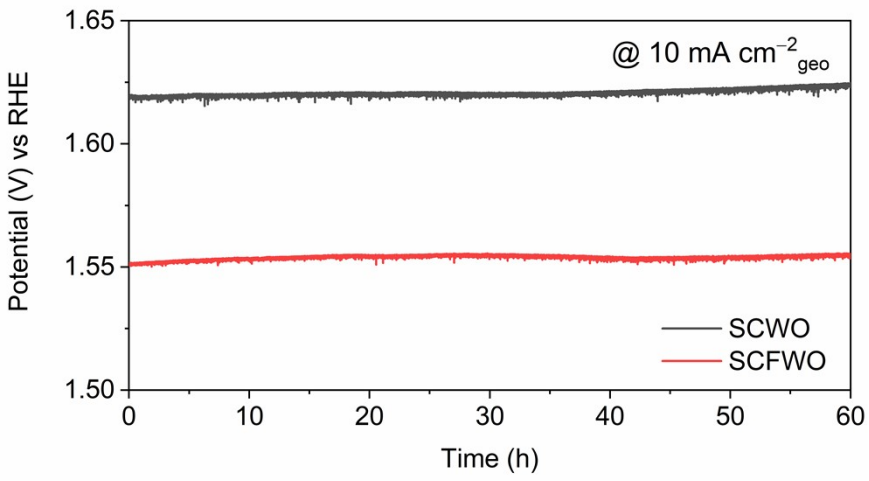

Supplementary Fig. 10. Chronopotentiometry (CP) measurements on the SCWO and SCFWO samples at 10 mA cm^{-2}_{geo} for 60 hours.

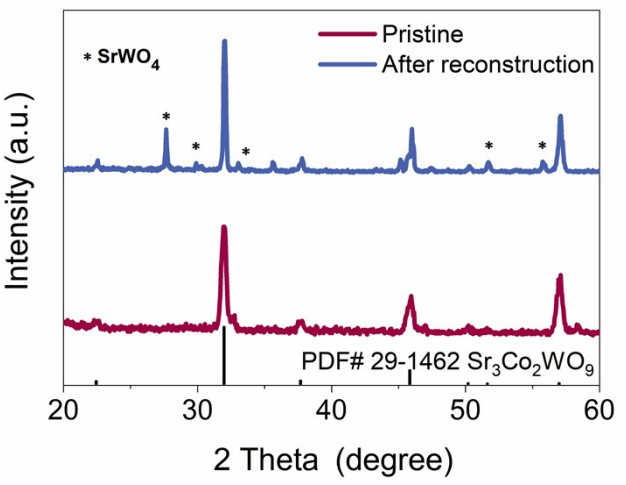

Supplementary Fig. 11. PXRD patterns of SCFWO samples before and after undergoing thermal activation at 60 ℃.

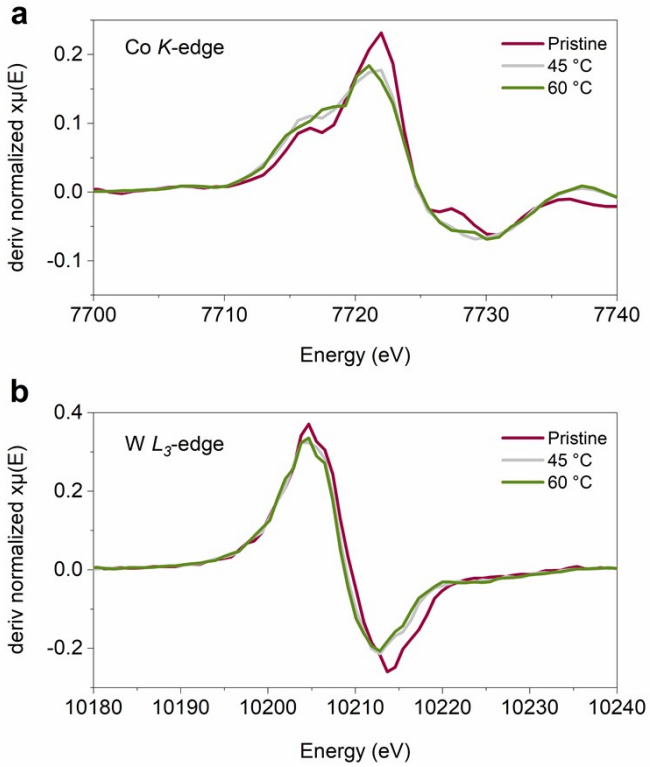

Supplementary Fig. 12. (a) First derivative for the normalized Co *K*-edge XANES spectra of pristine SCFWO samples and after been thermally activated at 45 ℃ and 60 ℃. (b) First derivative for the normalized W L_3-edge XANES spectra of pristine SCFWO samples and after undergoing thermally activated at 45 ℃ and 60 ℃.

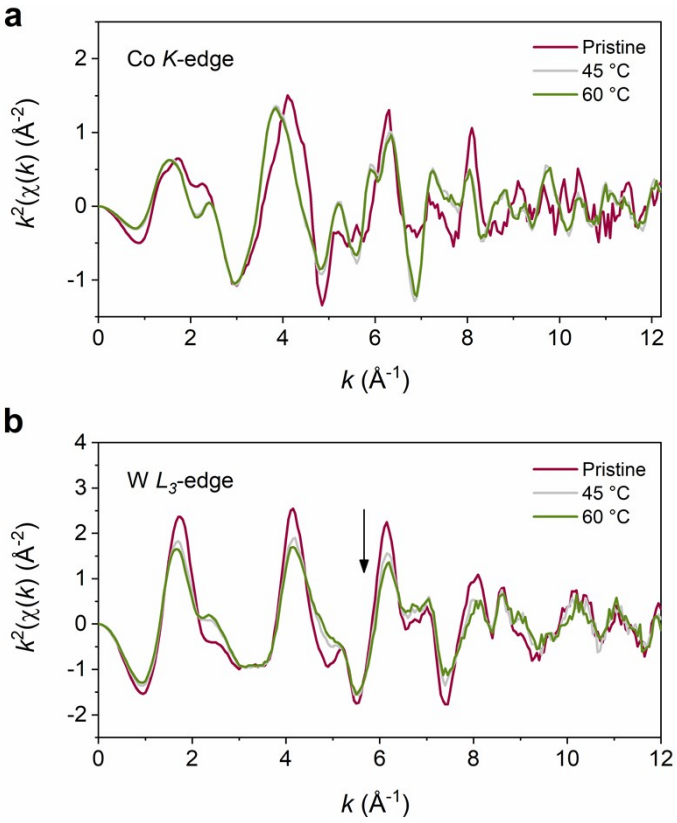

Supplementary Fig. 13. (a) *k*-space Co *K*-edge XAS spectra of pristine SCFWO samples and after been thermally activated at 45 ℃ and 60 ℃. (b) *k*-space W L_3-edge XAS spectra of pristine SCFWO samples and after undergoing thermally activated at 45 ℃ and 60 ℃.

As shown in the *k* space XAS spectra, all these data exhibited a high signal-to-noise ratio, ensuring reliable analysis of the EXAFS data. Additionally, the gradual decrease in oscillation amplitude observed in Fig. S13b demonstrates the reduction of long-range order in the perovskite sample during the thermal activation reconstruction process.

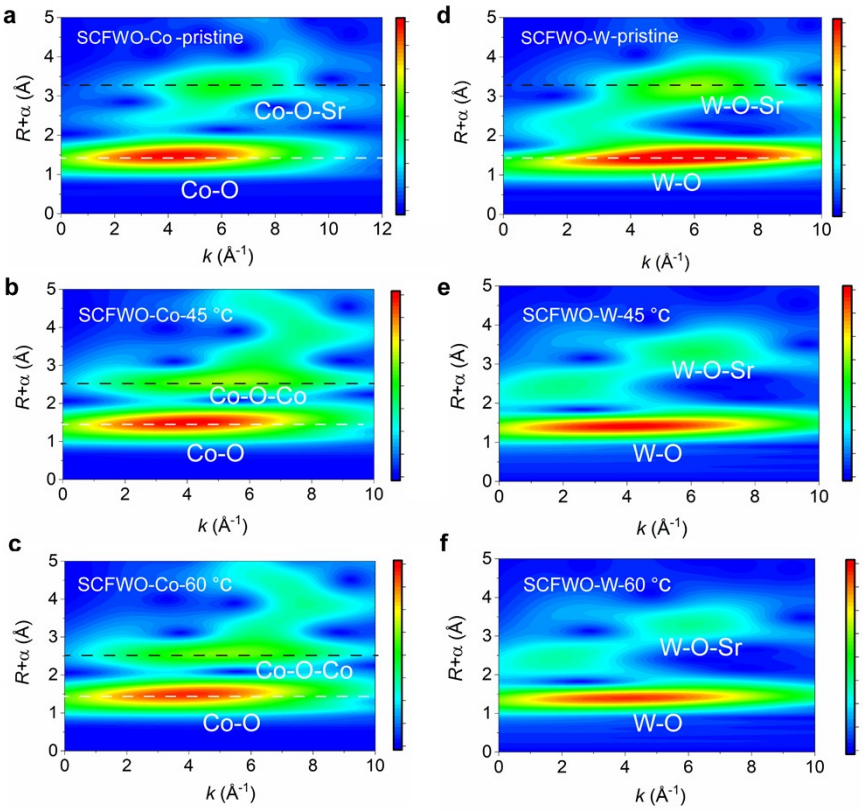

Supplementary Fig. 14. (a-c) Wavelet transform (WT) of k^2 weighted Co *K*-edge EXAFS data of pristine SCFWO samples and after been thermally activated at 45 ℃ and 60 ℃. (d-f) WT of k^2 weighted W L_3-edge EXAFS data of pristine SCFWO samples and after been thermally activated at 45 ℃ and 60 ℃.

Table S1. EXAFS fitting parameters and results for the Co *K*-edge EXAFS spectra of SCWO, SCFWO, and Co_3O_4 samples.

Sample	**Path**	**CN**	**σ^2 (Å^2)**	***R* (Å)**	***R*-factor**
SCWO-Co	Co-O	6 (fixed)	0.0074	2.037	0.015
□	□	□	□	□	□
□	□	□	□	□	□
SCFWO-Co	Co-O	6 (fixed)	0.0041	2.022	0.011
□	□	□	□	□	□
□	□	□	□	□	□
Co_3O_4-Co	Co_{tet}-O	4 (fixed)	0.0011	1.894	0.009
	Co_{oct}-O	6 (fixed)	0.001	1.946	

CN, coordination number; *R*, distance between absorbing and backscattering atoms; σ^2, Deby Waller factor to account for thermal and structural disorders; *R* factor as a measure of the goodness of fit. Co_{tet}-O, Co-O distance for the tetragonal site Co. Co_{oct}-O, Co-O distance for the octahedral site Co atom.

References

1. C. Wu, X. Wang, Y. Tang, H. Zhong, X. Zhang, A. Zou, J. Zhu, C. Diao, S. Xi, J. Xue and J. Wu, Origin of surface reconstruction in lattice oxygen oxidation mechanism based-transition metal oxides: A spontaneous chemical process, *Angew. Chem. Int. Ed.,* 2023, **62**, 202218599.
2. C. C. L. McCrory, S. Jung, J. C. Peters, and T. F. Jaramillo, Benchmarking heterogeneous electrocatalysts for the oxygen evolution reaction. *J. Am. Chem. Soc.,* 2013, **135**, 16977–16987.
3. Y. Du, Y. Zhu, S. Xi, P. Yang, H. O. Moser, M. B. H. Breese, A. Borgna, XAFCA: A new XAFS beamline for catalysis research. *J. Synchrotron Radiat.,* 2015, **22**, 839–843.
4. Ravel, B. and M. Newville, ATHENA, ARTEMIS, HEPHAESTUS: Data analysis for X-ray absorption spectroscopy using IFEFFIT. *J. Synchrotron Radiat.,* 2005, **12**, 537–541.